Desalination and Water Treatment
www.deswater.com

doi: 10.5004/dwt.2023.29419

290 (2023) 170–176
April

Stability of surrounding rock in broken zone of the tunnel in rich water and mountains

Ruiyu Xu

The Engineering and Technical College, Chengdu University of Technology, Leshan 614000, China, email: xuruiyu2023@163.com

Received 28 May 2022; Accepted 18 August 2023

ABSTRACT

During the excavation of tunnels, many hazards caused by the fracture zone and groundwater seepage are often encountered. Studying the surrounding rock's stability in the fracture zone of the mountain's water-rich tunnels is thus crucial. The rock mass's seepage and stress fields were studied by using the seepage theory of rock mass and Darcy's rule in the experiment, and a hydraulic coupling model of porous continuum was constructed according to the coupling relationship between them. After that, the experiment used FLAC3D software to conduct three-dimensional numerical analysis of the tunnel, and analyzed the surrounding rock's stability under different conditions. The findings demonstrate that the model's error rate is just 0.16% and that the surrounding rock's stability is influenced by the excavation plan, main support, and grade of the surrounding rock. Therefore, the model considers various factors for tunnel excavation and can be applied to the prediction of actual mountain tunnel construction.

Keywords: Mountain tunnel; Water-rich fractured zone; Seepage theory of rock mass; Traffic network

1. Introduction

The construction of road traffic network often requires the excavation of tunnels, and subterranean space development and usage in depth [1,2]. However, our nation has many mountains, and the water-rich fracture zones of the mountains contain a lot of fragmented rock masses and groundwater [3]. During tunnel excavation, the interaction between fragmented rock mass and groundwater often causes disasters such as tunnel collapse and water gushing. These accidents not only slow down the construction speed, but also threaten the lives of construction workers [4]. Therefore, it is extremely necessary to study the stability of the surrounding rock in the broken zone of the tunnel in rich water and mountains. In the current research, some scholars put forward scientific rules such as seepage theory and Darcy's rule, and discussed the law of interaction between various positions in the rock mass [5]. However, although certain research results can be harvested, there are also major limitations. Therefore, in this experiment, a variety of factors in the tunnel excavation process were comprehensively considered. On this basis, a hydraulic coupling model of porous continuum was constructed, and modeling analysis was performed using FLAC3D software. The purpose of the experiment is to explore the effect of the surrounding rock's grade on the tunnel, the initial support and the construction scheme on its stability, and contribute to the mountain forest tunnel's real building forecast plan.

2. Related work

Numerous academics have contributed to the study of the stability of surrounding rock in recent years. Kerbati et al. [6] proposed a technical method based on rock mechanics and geotechnical engineering to discuss the behavior and stability of underground mine rock mass in view of the increasingly difficult and difficult conditions faced by underground mining. This method mainly uses geomechanics and

numerical methods to predict the stress distribution of the underground mine environment. The findings indicate that this method can effectively help solve rock mass stability problems. Gao et al. [7] found that random and hazy elements influence the stability of the surrounding rock, and the existing evaluation indicators have complex interactions. In order to increase the precision of surrounding rock stability assessment, they proposed a model for assessing the stability of the nearby rocks based on fuzzy rock engineering system. The model improves the credibility of indicator weights through the transformation of cloud theory, and can fully reflect the interactive relationship of indicators. The viability of the model has been confirmed through experiments. Based on the topic of deep basement excavation, a three-dimensional geomechanics model experiment was conducted by Zhang et al. [8]. According to the deep burial depth of the laboratory, the researchers developed a loading system with automated excavation tool and sophisticated numerical control feature. The system reveals the displacement and stress changes around the cave, providing important guidance for the underground excavation laboratory. Liu et al. [9] discovered that road driving, such as coal mining, often has an influence on large cross-sectional chamber groups, resulting in poor stability and difficult management of the surrounding rock. In response to the above phenomenon, the researchers investigated the evolution law of the triangular chamber group's surrounding rock under various stresses. The final experiment revealed that the oscillation amplitude of surrounding rock stress is strongly associated with the action of dynamic load. Su et al. [10] studied the support system of weak rock tunnel. In view of the characteristics that the support system of weak rock tunnel is often composed of artificial support structure and rock mass around the tunnel, they proposed a technique for calculating the safety factor of adjacent rock components and a stability analysis method of surrounding rock combined with artificial support. This technique seeks to measure the stable tunnel's minimal internal pressure as well as the stability limit deformation of the rock pair around the tunnel. The experiment finally verified the effectiveness of this method.

Currently, many scholars are discussing the research and application of the hydraulic coupling model in porous continuum. A novel fracture-pore mixed seepage model, which is primarily made up of a porous seepage model and a fracture seepage model, was suggested by Yan et al. [11]. The model guarantees the numerical accuracy and operating efficiency by calculating the uninterrupted node components' fluid exchange coefficient. It is applied to fix the fluid flow issue in the porous fractured medium, which verifies that the model has good practicability. Based on the Biot poroelastic model and the relationship between natural and hydraulic cracks [12] developed a game-changing computational paradigm for multiphase flow, geomechanics, and fracture modeling. The diffusion adaptive finite element phase field approach was used to conduct numerical simulations of natural and hydraulic fractures. The final experiment verified the effectiveness of the framework through numerical examples. Cusini et al. [13] captured the relationship between fluid flow and mechanics using an embedded discrete fracture model and an embedded finite element approach. The combination of these two methods can effectively reduce the geometric complexity. Experiments were performed to verify performance in heterogeneous storage scenarios involving complex crack distribution, and the results showed that the method showed good convergence and accuracy. To facilitate particle movement and deposition in porous media, Feng et al. [14] proposed a research method combining computational fluid dynamics and the discrete element approach are used together to explore the particle migration process in porous media. The Ergon equation and the DKT phenomenon are selected in experiments to test the efficacy of the suggested approach. The final findings indicate that when the concentration of particles increases, the particles will eventually occupy the pores, reducing porous medium permeability. Liu [15] proposed a strong discontinuity embedded approach and applied it to the investigation of the propagation of a single hydraulic fracture in poroelastic medium. The suggested approach primarily adds discontinuous deformation modes to the strain field, while allowing fracture to be modeled within the element. The experiment verifies the effectiveness and feasibility of the proposed method by comparing with the asymptotic analytical solution of single hydraulic fracture propagation.

In summary, the research on the rock's surrounding stability and the hydraulic coupling model of porous continuum has attracted the attention of researchers from all walks of life. This topic is closely related to people's daily life, so it is critical to investigate the rock's surrounding stability in the cracked zone of mountainous water tunnels. Aiming at the limitations of existing research in this field, this experiment combines Darcy's law and rock mass seepage hypothesis, and according to the coupling relationship between the two, a hydraulic coupling model of porous continuum is constructed to analyze the rock's surrounding stability.

3. Study on the stability of surrounding rock based on rock mass seepage theory

3.1. Coupling relationship between seepage field and stress field in rock mass

The structural structure of the rock mass is often more complex over the lengthy period of geological change as a result of weathering, erosion, and other factors [16]. In rock mass hydraulics, depending on the pore type of the aquifer's rock mass, the rock mass's supporting medium is generally divided into three types, namely, pore medium, fracture medium and dissolved cave medium [8], as shown in Fig. 1.

Among them, the structural planes of the fractured media are criss-crossed and contain fissure water. Solid, liquid and gas can exist in fractured media at the same time, which is the main type of rock mass in tunnel engineering [17,18]. In the fracture zone of a mountain range, the content of groundwater is relatively large, which is easy to soften the rock mass. The stability of a pile of rock is readily impacted by both hydrostatic and hydrodynamic pressure at the same time [19]. The principle of groundwater softening is as follows: groundwater dissolves and scours water-soluble substances in rock formations, changing the rock mass structure and reducing the shear strength [20]. The friction caused by the groundwater's hydrodynamic pressure when it begins to flow down the crack will affect

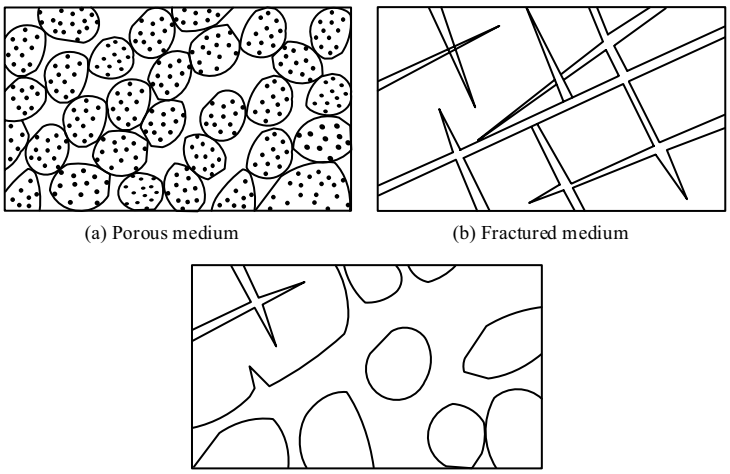

Fig. 1. Three media types of rock mass.

the rock mass's structural surface [21]. It is quite important to study the movement law of groundwater in rock mass, whether it is in the prevention of geological disasters or in the safety protection of tunnel engineering. Relevant scholars put forward the rock mass seepage theory and Darcy's law. Darcy's law is shown in Eq. (1).

$$v = \frac{q}{A} = -k \cdot i \tag{1}$$

where v represents the average velocity of water flow; q represents the average flow volume per second, that is, seepage flow; A represents the cross-sectional area; k denotes the permeability coefficient; i stands for the hydraulic gradient. In three-dimensional space, Darcy's law for seepage velocity along three directions is shown in Eq. (2).

$$\begin{cases} v_x = -k\dfrac{\partial H_x}{\partial_x} = -k \cdot i_x \\ v_y = -k\dfrac{\partial H_y}{\partial_y} = -k \cdot i_y \\ v_z = -k\dfrac{\partial H_z}{\partial_z} = -k \cdot i_z \end{cases} \tag{2}$$

where H_x, H_y, H_z, respectively represent the seepage head difference along the direction of x, y, and z. In order to confirm whether the movement of groundwater can adopt Darcy's law, the Reynolds index is used to judge it, as shown in Eq. (3).

$$R_e = \frac{vd}{2\eta} \tag{3}$$

where R_e is the Reynolds index, which d represents the average diameter of rock and soil particles, and η represents the kinematic viscosity coefficient of groundwater. When the Reynolds index is satisfied $1 \le R_e \le 10$, the groundwater movement can be characterized by Darcy's law, that is, the groundwater movement satisfies a linear relationship. Assuming that the frictional resistance between the water flow and the rock mass is not considered, after measuring the hydraulic gradient and viscous force balance, it is possible to determine the average water flow velocity in the crack, and the permeability coefficient of the fracture can be deduced from this, as shown in Eq. (4) shown.

$$k_f = -\frac{gb^2}{12v_m} \tag{4}$$

where b is the crack width. When the groundwater movement does not satisfy the linear relationship, there is Eq. (5).

$$v^m = -k'_f j \tag{5}$$

where k'_f represents the nonlinear permeability coefficient, m is the nonlinear index. To get the nonlinear flow formula of the fracture without friction resistance, multiply both sides of Eq. (5) by b^m simultaneously. Then, take the logarithmic simplification on both sides of the nonlinear flow formula simultaneously, and Eq. (6) can be obtained.

$$\lg j = \lg \frac{1}{k'_f b_m} + m \lg q \tag{6}$$

The change in stress will have an impact on the permeability of the rock mass, and the seepage coefficient tensor can be expressed by rock mass stress and rock mass seepage pressure, as shown in Eq. (7).

$$K_{ij} = K(\sigma, p) \tag{7}$$

Since the seepage movement of groundwater is three-dimensional, the permeability coefficients of groundwater flow in different directions and at different times are not the

same. As a result, the permeability coefficient tensor may be used to represent the permeability coefficient in each direction, as illustrated in Eq. (8).

$$K = \begin{bmatrix} k_{xx}k_{xy}k_{xz} \\ k_{yx}k_{yy}k_{yz} \\ k_{zx}k_{zy}k_{zz} \end{bmatrix} \tag{8}$$

The groundwater seepage activity will have an influence on how the stress field of the rock mass is distributed, which will also have an impact on the rock mass's structure. As the rock mass's structure changes, so too will its permeability, resulting in a dynamic equilibrium, as illustrated in Fig. 2.

Through the examination of their partnering connection, the law can be obtained. On the basis of the coupling relationship between the two, the appropriate models for calculating the distribution of the stress field and the seepage field may be developed, so as to better formulate and complete the tunnel construction plan.

3.2. Establishment of hydraulic coupling model in porous continuum

The rock mass is thought to be an equivalent continuous porous medium, and based on the coupling connection between the seepage field and the stress field, the hydraulic coupling model of the porous continuous medium is created, so as to study and examine the rock's stability in the water-rich fracture zone of the mountain tunnel [22]. One

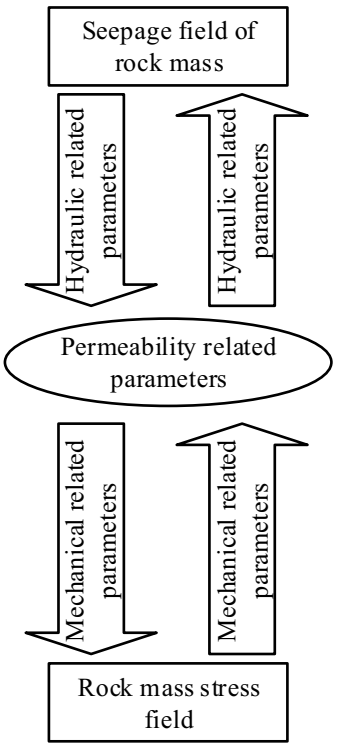

Fig. 2. Coupling relationship between stress field and seepage field.

of the most essential fluid calculation factors in the model is the permeability coefficient, and the surrounding rock's permeability coefficient in the water Rich fracture zone of the mountain tunnel is different from the surrounding rock's in general, as shown in Table 1.

Eq. (9) illustrates the link between the effective gap width, the density of the rock mass, and the permeability coefficient tensor.

$$\bar{K} = \frac{\gamma \bar{b}^3 \lambda}{12\mu} \begin{bmatrix} 1-\cos^2\alpha\sin^2\beta & -\sin\alpha\cos\alpha\sin^2\beta & -\cos\alpha\sin\beta\cos\beta \\ -\sin\alpha\cos\alpha\sin^2\beta & 1-\sin^2\alpha\sin^2\beta & -\sin\alpha\sin\beta\cos\beta \\ -\cos\alpha\sin\beta\cos\beta & -\sin\alpha\sin\beta\cos\beta & 1-\cos^2\beta \end{bmatrix} \tag{9}$$

where $\bar{K}$ denotes the permeability coefficient tensor, $\bar{b}$ is the effective gap width, λ is the rock mass's structural surface density, α, β are the inclination and inclination angle of the rock mass's fracture surface, respectively.

The structure of the rock and soil mass will vary throughout the tunnel excavation process owing to the involvement of human construction elements, and the seepage performance of the rock mass will also change appropriately. The fragmented media change may be separated into two parts: block deformation and fracture deformation, both of which conform to the characteristics of elastic deformation. The elastic strain tensor of the fractured rock medium is shown in Eq. (10).

$$\varepsilon_{ij} = \varepsilon_{ij}^{(m)} + \varepsilon_{ij}^{(c)} \tag{10}$$

where $\varepsilon_{ij}^{(m)}$ refers to the rock block's distortion. $\varepsilon_{ij}^{(c)}$ represents the deformation of the crack. If K_n is the normal stiffness of the crack, there is Eq. (11).

$$\overline{K_n} = \int_\Omega K_n E(n) a\Omega = \frac{a_1 + \xi\sigma_{ij}N_{ij}}{2r} \tag{11}$$

where $\overline{K_n}$ is the average value of fracture normal stiffness K_n in the whole space domain; the radius of the circular fracture is shown by r, a_1 is the Bandis experimental constant, σ_{ij} is the entire stress tensor of the rock-soil medium, and N_{ij} is the distribution geometry tensor of the crack. As a result of Eq. (11), the formula of the effective stress tensor of rock-soil medium, such as Eq. (12).

Table 1
Comparison of seepage field calculation parameters between surrounding rocks in the water-rich fractured zone of mountain tunnels and general surrounding rocks

Surrounding rock type	Permeability coefficient (cm/s)	Porosity (%)	Natural void ratio (%)
Broken zone surrounding rock	3.29×10^{-8}	0.26	0.59
General surrounding rock	1.03×10^{-7}	0.41	0.32

$$\sigma_{eij} = \sigma_{ij} - p\delta_{ij} \tag{12}$$

where the effective stress tensor of the rock-soil medium is denoted by σ_{eij}; p represents the groundwater seepage pressure of the rock-soil medium. Then the tangential stiffness of the crack can be expressed as the equation shown in Eq. (13).

$$K_s = \frac{50}{r}\sigma_n \tan\left[R_{ij}\log\left(\frac{S_{jc}}{\sigma_n}\right) + \theta_r\right] \tag{13}$$

where K_s denotes the crack's tangential stiffness, σ_n is the normal stress, θ_r represents the friction angle, the roughness coefficient of the fracture surface is denoted by R_{jc}. S_{jc} is the average value of the crack compressive strength. After acquiring the equivalent continuum's fracture strain tensor and elastic compliance tensor, as well as the rock block's elastic compliance tensor, the total strain tensor of the fracture in the equivalent continuum may be calculated, as shown in Eq. (14).

$$\varepsilon_{ij} = \varepsilon_{ij}^{(c)} + \varepsilon_{ij}^{(m)} \tag{14}$$

In Eq. (14), $\varepsilon_{ij}^{(c)}$ is the strain tensor of the fracture, $\varepsilon_{ij}^{(m)}$ is the elastic flexibility tensor of the fracture, and ε_{ij} is the fracture strain tensor. The corresponding continuum mathematical model of seepage field and stress field coupling may be formed by combining the aforementioned components, as indicated in Eq. (15).

$$\begin{cases} \beta_p\left(\dfrac{b_0}{2r}F_0 - \overline{a}_1 F_{ij}\sigma_{eij}\right)\dfrac{\partial p}{\partial t} - \dfrac{\partial}{\partial t}\left[\overline{a}_1 F_{ij}\left(\sigma_{eij} - p\delta_{ij}\right)\right] = \nabla\left[\dfrac{k_{ij}\sigma_{eij}}{\mu}\left(\nabla p + \rho g\nabla z\right)\right] \\ k_{ij}(\sigma_{eij}) = \lambda\left(A_{ss}\delta_{ij} - A_{ij}\right) \\ n(\sigma_{eij}) = \dfrac{b_0}{2r}F_0 - \overline{a}_1 F_{ij}\sigma_{eij} \end{cases} \tag{15}$$

The permeability of the rock mass itself is not included in the hydraulic coupling model of porous continuum; only the fractures of the rock mass are examined. After getting the preconditions, the model may be used to determine the stress and seepage pressure distributions and include them into the model to solve based on the coupling connection between the two.

4. Research on model performance and stability of tunnel surrounding rock

4.1. Accuracy of hydraulic coupling model in porous continuum

FLAC3D software was used to model and analyze the Xiaobeishan No. 1 Tunnel in X Province to explore the elements impacting the stability of the rock around the tunnel in the water-rich fracture zone of the mountains. The actual data of the Xiaobeishan No. 1 Tunnel were compared with the data predicted by the model to confirm the correctness of the hydraulic coupling model in porous continuum. The construction plan adopts the step method to excavate the tunnel. When there is a –10 m gap between the monitoring portion and the tunnel face, the real vault displacement and the model predicted vault displacement in different processes are shown in Table 2.

As may be seen in Table 2, in process 1, the predicted displacement of the model is consistent with the real displacement, and the error is 0; in process 3 and 4, the error is the largest, both differ from the real displacement by 0.02 mm, and the error rates are 0.36% and 0.22%; the model predicts that the average displacement error of the vault displacement in the six processes is 0.12 mm, and the average error rate is 0.16%. The aforementioned findings demonstrate that the hydraulic coupling model is very accurate and may be used to forecast the rock around the tunnel's stability.

4.2. Influence of support and surrounding rock grade on surrounding rock stability

In the FLAC3D software, the shell unit simulates and analyzes the tunnel's first support in order to examine the impact of the tunnel's initial support under various grades of surrounding rock. The tunnel surrounding rock grade is classified based on factors such as elastic modulus, Poisson's ratio, density, and permeability coefficient. The tunnel excavation technique employs the step approach consistently to improve the accuracy of the findings. The distance between the tunnel face and the monitoring section represents the progress of excavation. Fig. 3 depicts the distance between the monitoring section and the tunnel face as well as the change in the tunnel vault settlement distance.

Fig. 3 demonstrates that before the distance from the face of the tunnel –15 m, the arch's bottom uplift is zero relative to the surrounding rock's various grades, and after the distance of –10 m from the tunnel face, except for the surrounding rock of grade III, the surrounding rocks of other grades no matter how much Whether it is supported or not, it starts to bulge. The bottom of the arch starts to swell and the displacement is minimal around 5 m from the face of the tunnel when the grade III surrounding rock first appears, and the displacement is only 0.12 m when it is 30 m away from the tunnel face. The level III surrounding rock photos with support and those without support both exhibit the same ups and downs. The images of the two are almost coincident, indicating that the uplift displacement of the two is consistent and there is almost no change. This

Table 2
Model prediction data accuracy

Process	Real displacement (mm)	Model predicted displacement (mm)	Error (mm)	Error rate (%)
1	1.30	1.30	0	0
2	5.36	5.35	0.01	0.19
3	8.29	8.32	0.02	0.36
4	8.91	8.89	0.02	0.22
5	9.96	9.95	0.01	0.10
6	10.70	10.71	0.01	0.09

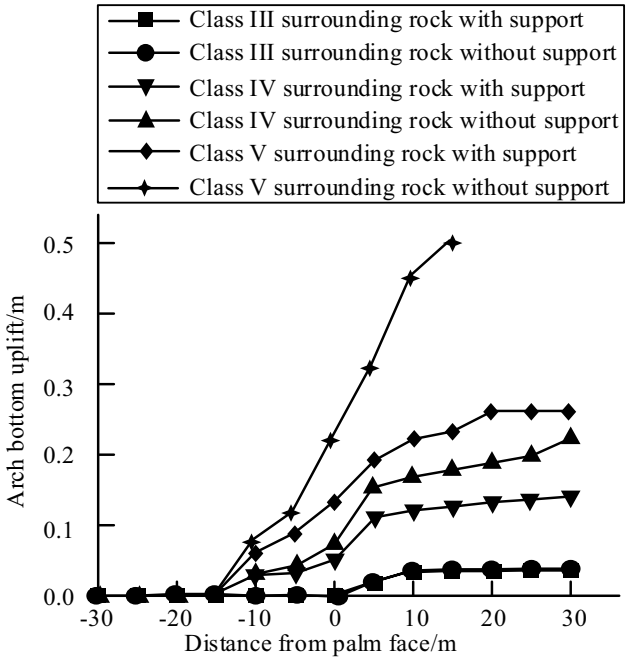

Fig. 3. Change of tunnel arch bottom.

situation also shows that the adjacent grade III rock itself is more stable. The grade IV and grade V rocks that surround it have a significant gap between them when they are supported and when they are not. Among them, the maximum displacement of the vault bottom uplift of grade IV surrounding rock is 0.15 m after support is added, and the maximum displacement without support is 0.23 m. The greatest displacement of the vault bottom, which is 0.25 m, occurs when the monitoring section is 30 m from the tunnel's face after the surrounding grade V rock has been stabilized. The displacement of the V-level surrounding rock reaches 0.5 m only when the monitoring part is 15 m from the tunnel's face without assistance. According to the aforementioned findings, the stability of the surrounding rock decreases with increasing slope. In addition, the neighboring rocks of grades IV and V lack sufficient stability, so initial support during excavation is very necessary.

4.3. Effects of different excavation methods on the stability of surrounding rock

The stability of the rock around the tunnel will be impacted by various tunnel excavation strategies in addition to the grade of the surrounding rock and its main support. To study the influence of different construction schemes on the stability of surrounding rock, three construction schemes of step method, core soil-step method and core soil method were used for simulation analysis. When the monitoring section's distance from the tunnel face is –10 m, the real vault displacement and the model predicted vault displacement of different processes in different schemes are shown in Fig. 4.

As shown in Fig. 4, the vault displacement of the core soil-step method and the core soil-step method are exactly the same before the fourth process because the core soil-step

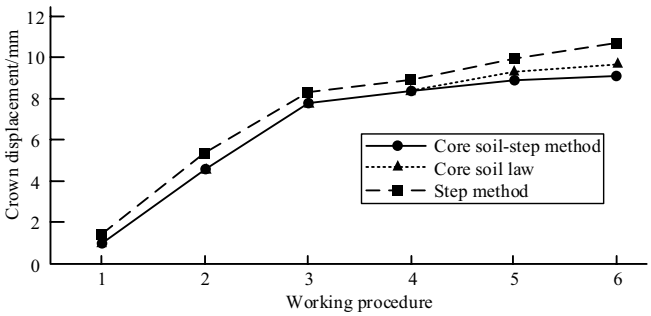

Fig. 4. Crown displacement of different schemes.

technique is consistent with the previous process of the core soil-step method. The vault displacement of the step method has been greater than that of the other two schemes since the first process; in the sixth process, the vault displacement of the step method reaches the maximum, which is 10.7 mm. The maximum vault displacements of core soil method and core soil-step method are 9.71 and 9.08 mm, respectively. The core soil-step technique has the least displacement distance, which is 1.62 and 0.63 mm smaller than the step method's and core soil method's maximum displacement, respectively. The above data demonstrate that the stability of the tunnel's surrounding rock is affected by numerous construction procedures, with the core soil-step approach having the least impact.

5. Conclusion

The investigation of the stability of the surrounding rock in the tunnel's fractured zone in rich water and mountains is the premise of the tunnel construction. Combining Darcy's law and rock mass seepage theory, a hydraulic coupling model of porous continuum was constructed, and FLAC3D software was used for modeling analysis. The findings indicate that the model has an average prediction error of 0.12 mm and a prediction error rate of 0.16%. The results demonstrate that the model may be used in real-world circumstances and has a high prediction accuracy. The grade III surrounding rock under the arch has a maximum displacement of 0.12 m. With assistance, grade IV surrounding rock can move up to 0.15 m; without support, it can move up to 0.23 m. When the monitoring section is 15 m from the tunnel wall without support, the maximum displacement of grade V surrounding rock is 0.25 m, and the maximum displacement of the arch floor is 0.5 m. The above situation demonstrates that the stability decreases as the surrounding rock grade increases. The results of simulation analysis of different schemes indicates that the shortest displacement distance is 9.08 mm for the core soil-step approach, which is 1.62 and 0.63 mm less than the maximum displacement of the step method and core soil method, respectively. This finding demonstrates that the core soil-step method has the least impact on the rock's surrounding stability. This finding demonstrates that the constructed model has good application prospects, and the tunnel's surrounding rock's stability is related to the grade of the surrounding rock and the construction plan. Meanwhile, the addition of primary support will also affect the surrounding rock's stability. This

research has some relevance for the building of mountain tunnels, however the permeability of the rock mass itself is not taken into account. Future study can improve on this.

References

[1] C. Zang, M. Chen, G. Zhang, K. Wang, D. Gu, Research on the failure process and stability control technology in a deep roadway: numerical simulation and field test, Energy Sci. Eng., 8 (2020) 2297–2310.

[2] H. Fan, L. Li, H. Liu, S. Shi, J. Hu, S. Zhou, Advanced stability analysis of the tunnels in jointed rock mass based on TSP and DEM, KSCE J. Civ. Eng., 25 (2021) 1491–1503.

[3] D. Song, X. Liu, Z. Chen, J. Chen, J. Cai, Influence of tunnel excavation on the stability of a bedded rock slope: a case study on the mountainous area in southern Anhui, China, KSCE J. Civ. Eng., 25 (2021) 114–123.

[4] Z. Liang, R. Xue, N. Xu, L. Dong, Y. Zhang, Analysis on microseismic characteristics and stability of the access tunnel in the main powerhouse, Shuangjiangkou hydropower station, under high in situ stress, Bull. Eng. Geol. Environ., 79 (2020) 3231–3244.

[5] H. Jing, J. Wu, Q. Yin, K. Wang, Deformation and failure characteristics of anchorage structure of surrounding rock in deep roadway, Int. J. Min. Sci. Technol., 30 (2020) 593–604.

[6] N.R. Kerbati, L. Gadri, R. Hadji, A. Hamad, M.L. Boukelloul, Graphical and numerical methods for stability analysis in surrounding rock of underground excavations, example of Boukhadra Iron Mine N.E Algeria, Geotech. Geol. Eng., 38 (2020) 2725–2733.

[7] Y. Gao, F. Gao, K. Zhou, Evaluation model of surrounding rock stability based on fuzzy rock engineering systems (RES)-connection cloud, Bull. Eng. Geol. Environ., 79 (2020) 3221–3230.

[8] Q. Zhang, C. Liu, K. Duan, Z. Zhang, W. Xiang, True three-dimensional geomechanical model tests for stability analysis of surrounding rock during the excavation of a deep underground laboratory, Rock Mech. Rock Eng., 53 (2020) 517–537.

[9] X. Liu, S. Song, Y. Tan, D. Fan, J. Ning, X. Li, Y. Yin, Similar simulation study on the deformation and failure of surrounding rock of a large section chamber group under dynamic loading, Int. J. Min. Sci. Technol., 31 (2021) 495–505.

[10] Y. Su, Y. Su, M. Zhao, N. Vlachopoulos, Tunnel stability analysis in weak rocks using the convergence confinement method, Rock Mech. Rock Eng., 54 (2021) 559–582.

[11] C. Yan, H. Fan, D. Huang, G. Wang, A 2D mixed fracture–pore seepage model and hydromechanical coupling for fractured porous media, Acta Geotech., 16 (2021) 3061–3086.

[12] S. Lee, M.F. Wheeler, Modeling interactions of natural and two-phase fluid-filled fracture propagation in porous media, Comput. Geosci., 25 (2021) 731–755.

[13] M. Cusini, J.A. White, N. Castelletto, R.R. Settgast, Simulation of coupled multiphase flow and geomechanics in porous media with embedded discrete fractures, Int. J. Numer. Anal. Methods Geomech., 45 (2021) 563–584.

[14] Q. Feng, L. Cha, C. Dai, G. Zhao, S. Wang, Effect of particle size and concentration on the migration behavior in porous media by coupling computational fluid dynamics and discrete element method, Powder Technol., 360 (2020) 704–714.

[15] F. Liu, Modeling hydraulic fracture propagation in permeable media with an embedded strong discontinuity approach, Int. J. Numer. Anal. Methods Geomech., 44 (2020) 1634–1655.

[16] J. Li, The coal pillar design method for a deep mining roadway based on the shape of the plastic zone in surrounding rocks, Arabian J. Geosci., 13 (2020) 454, doi: 10.1007/s12517-020-05501-9.

[17] F.-q. Gong, W.-x. Wu, T.-b. Li, Simulation test of spalling failure of surrounding rock in rectangular tunnels with different height-to-width ratios, Bull. Eng. Geol. Environ., 79 (2020) 3207–3219.

[18] D.-y. Fan, X.-s. Liu, Y.-l. Tan, S.-l. Song, J.-g. Ning, Q. Ma, Numerical simulation research on response characteristics of surrounding rock for deep super-large section chamber under dynamic and static combined loading condition, J. Cent. South Univ., 27 (2020) 3544–3566.

[19] J. Zhang, State of art and trends of rock slope stability with soft interlayer, J. Eng. Geol., 28 (2020) 626–638.

[20] Z. Hu, N. Xu, B. Li, Y. Xu, J. Xu, K. Wang, Stability analysis of the arch crown of a large-scale underground powerhouse during excavation, Rock Mech. Rock Eng., 53 (2020) 2935–2943.

[21] M. Hu, J. Rutqvist, Multi-scale coupled processes modeling of fractures as porous, interfacial and granular systems from rock images with the numerical manifold method, Rock Mech. Rock Eng., 55 (2022) 3041–3059.

[22] X. Yan, H. Sun, Z. Huang, L. Liu, P. Wang, Q. Zhang, J. Yao, Hierarchical modeling of hydromechanical coupling in fractured shale gas reservoirs with multiple porosity scales, Energy Fuels, 35 (2021) 5758–5776.